ADVANCED QUANTUM TECHNOLOGIES
www.advquantumtech.com

Plug&Play Fiber-Coupled 73 kHz Single-Photon Source Operating in the Telecom O-Band

Anna Musiał, Kinga Żołnacz, Nicole Srocka, Oleh Kravets, Jan Große, Jacek Olszewski, Krzysztof Poturaj, Grzegorz Wójcik, Paweł Mergo, Kamil Dybka, Mariusz Dyrkacz, Michał Dłubek, Kristian Lauritsen, Andreas Bülter, Philipp-Immanuel Schneider, Lin Zschiedrich, Sven Burger, Sven Rodt, Wacław Urbańczyk, Grzegorz Sęk, and Stephan Reitzenstein**

A user-friendly, fiber-coupled, single-photon source operating at telecom wavelengths is a key component of photonic quantum networks providing long-haul, ultra-secure data exchange. To take full advantage of quantum-mechanical data protection and to maximize the transmission rate and distance, a true quantum source providing single photons on demand is highly desirable. This great challenge is tackled by developing a ready-to-use semiconductor quantum-dot-based device that launches single photons at a wavelength of 1.3 μm directly into a single-mode optical fiber. In the proposed approach, the quantum dot is deterministically integrated into a nanophotonic structure to ensure efficient on-chip coupling into a fiber. The whole arrangement is integrated into a 19″ compatible housing to enable stand-alone operation by cooling via a compact Stirling cryocooler. The realized source delivers single photons with a multiphoton events probability as low as 0.15 and a single-photon emission rate of up to 73 kHz into a standard telecom single-mode fiber.

1. Introduction

Sources of single photons (SPSs) are fundamental building blocks for photonic quantum technology, for example, secure quantum communication,[1,2] quantum internet,[3] and linear quantum computation.[4,5] Recent world-wide activities on the implementation of quantum networks,[6–11] including a satellite node,[12] reflect the importance of the field. Among different SPS concepts, to date, the purest single-photon emission is provided by semiconductor quantum dots (QDs) featuring probabilities of multiphoton events as low as 10^{-5} for emission wavelengths below 1 μm[13] (excluding their use for long-haul transmission),[14–16] and 10^{-4} at telecom wavelengths under non-resonant excitation.[17] Thus QDs constitute superb

Dr. A. Musiał, O. Kravets, Prof. G. Sęk
Laboratory for Optical Spectroscopy of Nanostructures
Department of Experimental Physics
Wrocław University of Science and Technology
Wybrzeże Wyspiańskiego 27, Wrocław 50-370, Poland
E-mail: anna.musial@pwr.edu.pl

K. Żołnacz, J. Olszewski, Prof. W. Urbańczyk
Department of Optics and Photonics
Wroclaw University of Science and Technology
Wybrzeże Wyspiańskiego 27, Wrocław 50-370, Poland

N. Srocka, J. Große, Dr. S. Rodt, Prof. S. Reitzenstein
Institute of Solid State Physics
Technische Universität Berlin
Hardenbergstraße 36, Berlin 10623, Germany
E-mail: stephan.reitzenstein@physik.tu-berlin.de

The ORCID identification number(s) for the author(s) of this article can be found under https://doi.org/10.1002/qute.202000018

DOI: 10.1002/qute.202000018

K. Poturaj, Dr. G. Wójcik, Dr. P. Mergo
Laboratory of Optical Fibers Technology
Institute of Chemical Sciences
Faculty of Chemistry
Maria Curie Sklodowska University
Maria Curie Sklodowska Sq. 3, Lublin 20-031, Poland

K. Dybka, M. Dyrkacz, Dr. M. Dłubek
Fibrain Sp. z o.o.
Zaczernie 190F, Zaczernie 36-062, Poland

K. Lauritsen, A. Bülter
PicoQuant GmbH
Rudower Chaussee 29, Berlin 12489, Germany

Dr. P.-I. Schneider, Dr. L. Zschiedrich, Dr. S. Burger
JCMwave GmbH
Bolivarallee 22, Berlin 14050, Germany

Dr. S. Burger
Zuse Institute Berlin
Takustraße 7, Berlin 14195, Germany

quantum emitters in terms of scalability, integration, and compatibility with advanced semiconductor technology.[18–25] A general drawback hindering real-world applications of In(Ga)As QDs is the cryogenic operation temperature. In fact, this is the main reason why commercially available quantum key distribution systems and experimental quantum networks are almost exclusively based on sources utilizing spontaneous parametric down conversion or attenuated lasers.[7–12,26–28] This is despite the drawbacks that the former is probabilistic with low efficiency, whereas the latter does not inherently provide single photons making transmission susceptible to the photon number splitting attack.[29]

In this work, we focus on developing a user-friendly SPS for quantum communication in the telecom O-band. This spectral window features a local minimum of loss in silica fibers, zero dispersion, and is suitable for multiplexing with C-band classical signals, without the need for expensive dark fibers for the quantum channel, due to good spectral isolation reducing Raman scattering. Interestingly, fiber-based quantum links have already been implemented using QDs at the telecom O-band by KTH Stockholm and by Toshiba-Cambridge.[30] However, in all these reports, the source was operated in complex and bulky experimental setups with QD emission coupled externally to a fiber. In order to take the application of QDs in quantum technologies to the next level, we developed a user-friendly "plug&play" QD SPS that is fiber-coupled, compact, and portable; includes a cooling system; and provides a stable train of spectrally filtered single photons in the O-band via a standard telecommunication single-mode fiber. Importantly, this source is very convenient for the end user as it does not require any adjustment and is fully operational after a 15 min cool-down cycle. In contrast, commercially available QD-based sources[31] utilize a standard bulky and expensive experimental cryostat and proof-of-principle realizations of compact designs[32] are multimode fiber-coupled. Moreover, both approaches operate at shorter wavelengths below 1 μm and require external spectral filtering of the single QD emission. A previous work reporting on a plug&play-like SPS operating in the telecom O-band[14] is based on the random positioning of a single-mode fiber bundle with respect to a regular non-deterministic micropillar array featuring 30% multiphoton events. Whereas in our case, the QD-mesa fabrication technology and the positioning of the fiber with respect to the mesa are fully deterministic, which allow for the utilization of a single-mode fiber and the integration with a highly efficient spectral filtering system. Overall, this is far beyond what has been reported so far in the field.

2. Results

2.1. Approach and Design

Our concept for the realization of a compact fiber-coupled, single-photon source is presented in **Figure 1**a. The overall scheme aims at providing the end user with a stable source of internally or externally triggered 1.3 μm single photons directly in a standard single-mode fiber. The source is easy to handle and operates at stable photon flux without the need of any alignment or additional spectral filtering, and can be further used, for example, for implementing quantum communication or computation schemes.

The frame in the scheme marks elements that are placed in a 19″ compatible housing shown in the image in Figure 1b. The desired functionality is realized in the following way: emission of the pulsed (80 MHz, pulse length <50 ps), non-resonant (805 nm), fiber-coupled, electrically triggered, semiconductor diode laser is first spectrally filtered to transmit only the laser line itself into the fiber arrangement. The laser filter avoids unwanted broadband emission background, for example, spontaneous emission from the laser cavity at the fiber output of our quantum device. In fact, while broad background emission (typically in the range of 600–1600 nm) from the laser is too low to efficiently excite QDs, it is comparable to the single QD signal. Therefore, it is crucial to filter this background out directly after the excitation laser. Once background emission passes the pumping filter in the all fiber configuration, it would not be filtered out by any other component and it would be spectrally integrated by the single-photon detectors into the photon flux. In that case, even the low, spectrally broad laser background could result in a total number of photons exceeding the number of photons from a single optical QD transition and therefore would make the whole system completely unusable. The spectrally filtered, single-mode laser signal is delivered to the sample via a reflection channel (see Figure 1a) of a specially designed three-port filter for pumping. The aforementioned fiber components are based on standard telecom fibers and they are spliced to a high numerical aperture fiber (numerical aperture (NA) = 0.42), which is precisely positioned with respect to the single-photon emitter via a recently developed interferometric method[33] with an alignment accuracy of 50 nm and fixed to the sample surface by low temperature compatible epoxy glue (see Experimental Section for details). It is important for a potential commercialization of our concept to perform not only the fiber alignment in a deterministic way, but also the device fabrication itself. For that, we apply in situ electron-beam lithography to preselect suitable QDs via cathodoluminescence mapping before integrating them into microstructures with a process yield >90% and a positioning accuracy of about 40 nm.[34] This way, cylindrical mesas were deterministically fabricated around preselected QDs in ≈20 μm × 20 μm writing fields (see inset to Figure 1c). In addition, the writing fields act as apertures and facilitate the orientation on the sample surface by mapping of its topography via a fiber in the alignment step. An exemplary cathodoluminescence map is shown in Figure 1c with the corresponding emission intensity color-coded for a narrow spectral range corresponding to the target wavelength of 1293–1295 nm at 40 K.[34] The position of the selected QD for device processing is marked by a black circle in Figure 1c. It is characterized by emission in the spectral range of interest, high intensity, and good spatial separation, which indicates that it originates from a single QD. This preselected QD is deterministically integrated into a cylindrical mesa with a diameter of 1090 ± 50 nm. Emission from this QD-micromesa is collected via the high-NA fiber and enters a transmission channel of the pumping filter that at the same time filters out the excitation signal. Finally, the target excitonic line of the QD is spectrally selected from emission of other QD transitions such as the biexciton via a narrow (0.6 nm) fiber-integrated band-pass filter. The exit port of this filter is connected to the FC/PC fiber connector at the optical output of our stand-alone single-photon source. The sample design, the microstructure, and fiber geometry, as well as the placement of

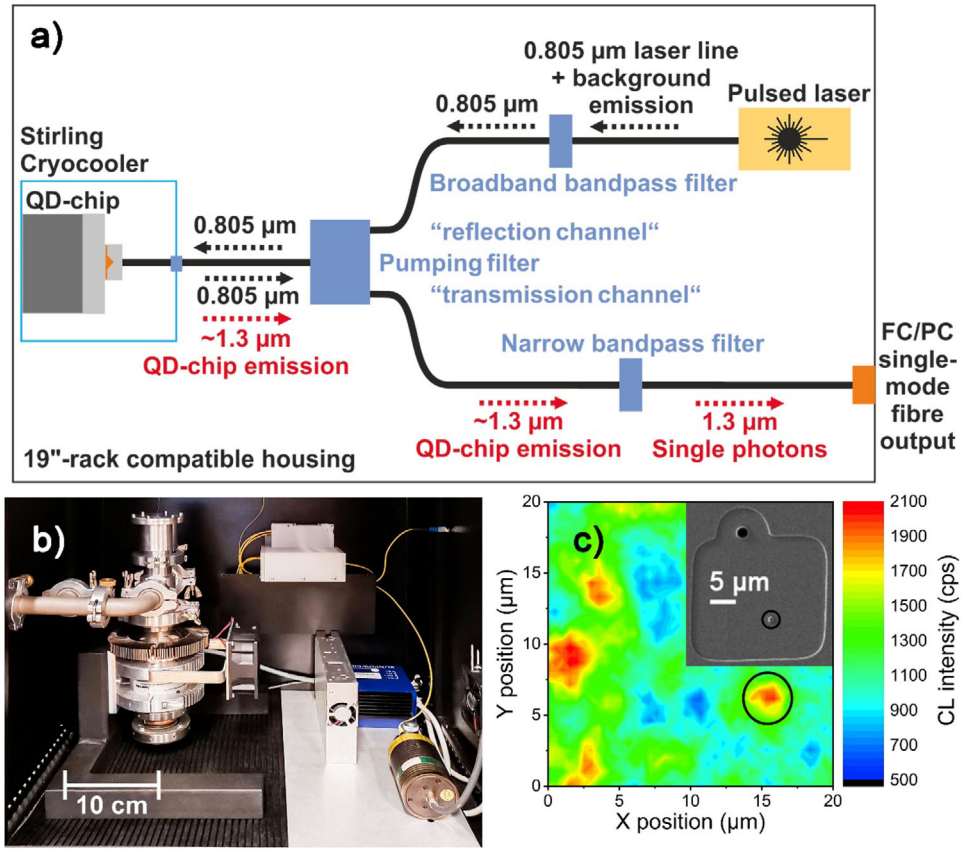

Figure 1. a) Scheme of the fully fiber-coupled single-photon source—the frame marks the device with a standard telecom single-mode FC/PC fiber connector as output. b) Image of the actual device with Stirling cryocooler on the left, pulsed excitation laser on the bottom-right, and the fiber components secured on the back wall. The ventilation openings in the housing and extra fans provide air flow for cooling of the Stirling cryocooler, which is operated in vertical position and mounted to the metal frame. c) Active region and sample patterning: spatial low-temperature (15 K) cathodoluminescence map in the spectral range corresponding to the target wavelength (1293–1295 nm) with the emission intensity color-coded and the target QD marked by a black circle. Inset: SEM image of the patterned sample with a mesa etched at the position of the target QD marked by a black circle.

the fiber follow the results of numerical optimization of the design parameters. To this end, the propagation of the light emitted by the QD was simulated using a finite-elements method.[35] The system parameters with optimal fiber-coupling efficiency were determined using Bayesian optimization as global optimization method.[36]

One of many technological challenges in implementing our device concept is the filtering of all spurious spectral contributions besides the single photons originating from the target QD transition from the all-fiber coupled system. This is realized by customized fiber components described in detail below. These optical elements have to provide high spectral isolation of the target QD transition with minimum insertion loss.

2.2. Specialty Fiber Components

Customized fiber components were designed and fabricated to fulfill the requirements of the stand-alone SPS device concept. Their optical characteristics (see **Figure 2**) were evaluated using a supercontinuum light source and an optical spectrum analyzer (OSA). The laser filter responsible for cleaning preliminarily the laser spectrum (see Figure 2a) has high transmission at the laser line wavelength (805 nm) of –2.5 dB and high attenuation in the spectral range of the QD emission (–62 dB). For the flexibility of the optical excitation, this filter is a broad band-pass to allow for application of different laser wavelengths in the range of 700–1000 nm. Laser light in this range is spectrally removed in the transmission channel (Figure 2c) of the fiber pumping filter with an optical isolation better than –35 dB in the broad range and better than –40 dB at the actual laser line position. In the final device, the laser attenuation was increased to >80 dB by combining two filters of this type. The results of the measurements are shown for a single filter due to limited dynamic range of the OSA. This channel exhibits high transmission for the optical signal from the QD with –0.7 dB loss above 1150 nm up to at least 1700 nm (OSA detection limit) covering both the telecom O-band and C-band. In the reflection channel, the transmission is high in the range above 750 nm (loss lower than –4.2 dB, see Figure 2b) so that the optical excitation can be delivered efficiently to the sample. The relatively high loss at the wavelength of the laser line is not an issue in the case of single QDs as for the investigated structures the emission is typically saturated at average excitation powers in the single µW range (cf. **Figure 3**b). The next step is to isolate a single optical transition from the other emission signals related to the wetting layer, strain reducing layer, possible

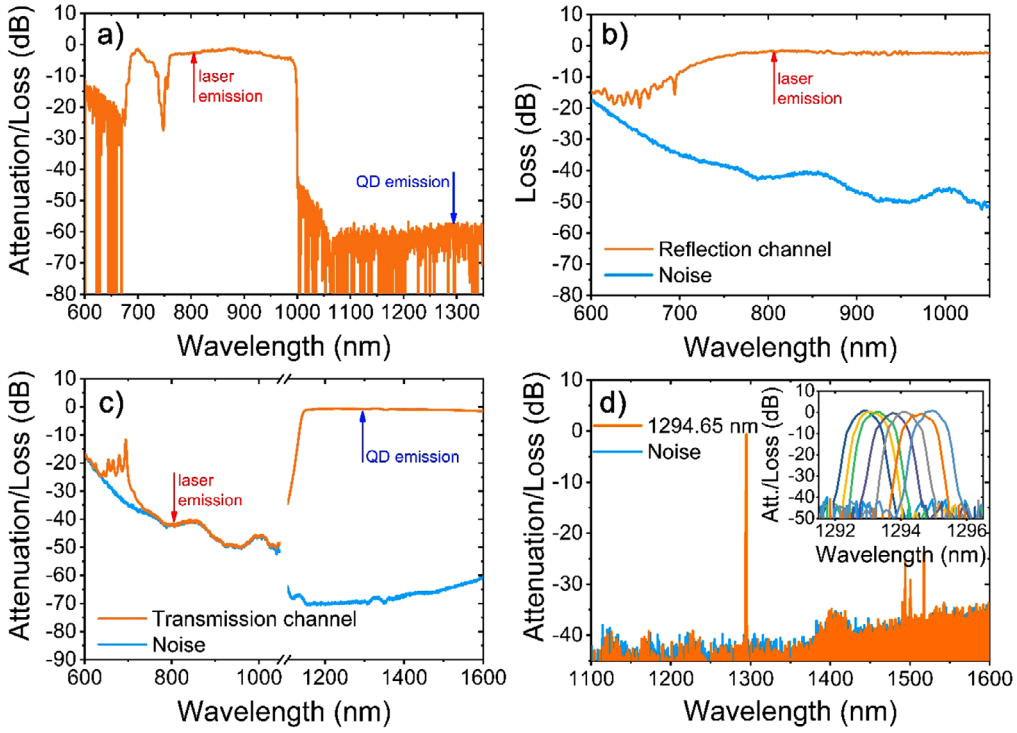

Figure 2. Spectral characteristics of the fiber components measured with a supercontinuum light source and an OSA: a) Broad band-pass filter for the excitation laser. b) Single-mode pumping filter—reflection channel through which the optical excitation is delivered to the sample after cleaning up its spectrum with the filter presented in (a). c) Single-mode pumping filter—transmission channel through which the QD signal is delivered to the detection system. The laser radiation is blocked by –40 dB. d) Single-mode narrow band-pass flat-top filter (0.6 nm full width at half maximum) with a central wavelength of 1294.65 nm; inset: set of fiber-based narrow band-pass filters differing in the adjustable central wavelength covering a 2 nm spectral range of 1293–1295 nm. All panels: The orange curves show the transmission of the investigated component with respect to the reference signal level and the blue ones depict the OSA noise level.

defects, or other excitonic complexes confined in the same QD. This functionality is realized by an ultra-narrow, top-flat, fiber-integrated band-pass filter (0.6 nm) (see Figure 2d). To provide some spectral flexibility, a set of seven exchangeable filters covering a wavelength range of 1293–1295 nm in the O-band with isolation better than –45 dB was fabricated.

2.3. Device Performance

The optical properties of the stand-alone telecom single-photon source are evaluated using a fiber-based Hanbury Brown and Twiss configuration equipped with superconducting nanowire single-photon photon detectors (SNSPDs). Figure 3a depicts the corresponding coincidences' histogram (black curve) obtained under pulsed excitation at 80 MHz with an average excitation power of 0.75 μW recorded at the laser input of the customized fiber arrangement ($T = 40$ K), which corresponds to 0.65 μW incident on the sample. The measured histogram was fitted by the sum of double-sided exponential decays for each maximum[17] including the background level in between the emission pulses. The peak height for the non-zero delay peaks determined from the fitting procedure was further used to normalize the coincidence events histogram to obtain the time delay-dependent second-order correlation function $g^{(2)}(\tau)$. The probability of multiphoton emission events $g^{(2)}(0)$ was determined from the fitting procedure as the ratio of the height of the central (zero delay) peak and the peaks at the long time delays and yields background-corrected $g^{(2)}(0) = 0.15 \pm 0.05$ proving single-photon emission from the target optical transition. Here, the level of uncorrelated background determined in between the emission pulses is subtracted from the as measured $g^{(2)}(0)$ (see Experimental Section for details). This uncorrelated background signal is mainly attributed to non-ideal laser suppression in the full-fiber configuration. This issue can most probably be resolved by further increasing the attenuation of the laser blocking filter in the future. The associated photoluminescence (PL) spectrum of the QD at the output of the SPS is shown in the inset of Figure 3a. The emission is centered at 1294.7 nm, and the linewidth equals 0.43 nm which is a typical value for 1.3 μm QDs,[18,37] where the quite significant inhomogeneous broadening is related mainly to spectral diffusion effects in the case of non-resonant excitation. At this excitation strength, the total photon flux yields 31 kHz at the device output which, taking into account the 15% probability of multiphoton events, corresponds to a true single-photon rate of 27 kHz (Figure 3b) according to the study by Pelton et al.[38] These rates were obtained by measuring the demonstrator's output using an external detection system and by correcting it for the detection system's efficiency. Therefore, this is the actual single-photon rate that the end user will be provided with. Under these excitation conditions, the probability of the source to emit a single photon per excitation pulse is in the range of

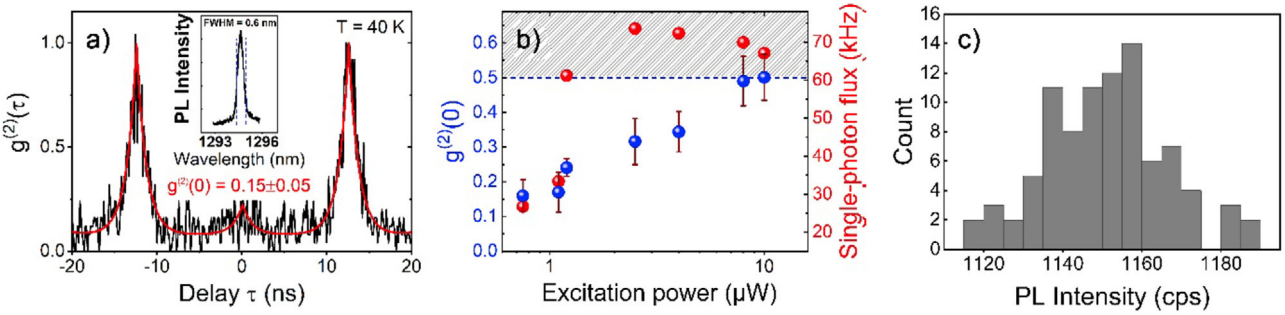

Figure 3. Optical properties of the stand-alone SPS: a) Normalized coincidences histogram measured under pulsed non-resonant excitation (0.75 μW average power at 80 MHz) in all-fiber configuration at $T = 40$ K (black curve) together with a fitting curve (red); inset: corresponding spectrum measured in all-fiber configuration including the fiber-based narrow band-pass filter (its bandwidth is marked with the dashed vertical lines). b) $g^{(2)}(0)$ (left scale, blue symbols) and single-photon flux rate at the output of the demonstrator (right scale, red symbols), measured under pulsed non-resonant excitation at $T = 40$ K as a function of average excitation power; the blue dashed line marks the $g^{(2)}(0) = 0.5$ defining the limiting value for single-photon operation; the error bars were obtained as the sum of the errors of fitting parameters. c) Stability test of the SPS: histogram of the count rates (averaged over 10 min) on one of the SNSPDs measured for 18 h. A statistical analysis yields a mean value of 1151 counts per second (cps) and a standard deviation of 16 cps that corresponds to a relative standard deviation of 0.014.

1%. This value is limited by a combination of below-saturation excitation, non-ideal internal quantum efficiency of the emitter, non-ideal coupling efficiency into the fiber, and losses of the all-fiber configuration as we discuss in Section 3 in more detail.

To investigate the upper limit of the achievable single-photon flux in the present device, coincidences histograms were measured as a function of the average excitation power in the range of 0.75 μW up to 10 μW. The corresponding power dependences of $g^{(2)}(0)$—blue symbols and single-photon flux—red symbols, are presented in Figure 3b. The limit of single-photon emission ($g^{(2)}(0) = 0.5$) is observed at 10 μW excitation power, suggesting that at this excitation strength emission from the QD is already saturated, and that a further increase of the excitation power results in increased uncorrelated emission background overlapping spectrally with the QD line. The associated maximal true single-photon flux corresponding to the saturation of QD emission equals 73 kHz. Its excitation power dependence follows the emission intensity dependence of the single QD transition.

During collection of the histogram at a given excitation power, the photon count rate at the SNSPDs was monitored over 18 h to get an insight into the long-term stability of the output of the source. The SNSPD detector count rates were averaged over 10 min and combined to generate the histogram presented in Figure 3c. In comparison to the emission rates in Figure 3b, this rate is decreased by the efficiency of the external detection system, including fiber beam splitter, fiber connectors, and quantum efficiency of the detectors themselves. The statistical evaluation of these data yields a mean value of 1151 cps with a standard deviation of 16 cps, which corresponds to the relative standard deviation of 0.014. This shows that the long-term stability of the demonstrator output is better than 1.5%.

3. Discussion and Outlook

For optimized performance, InGaAs QDs need to be cooled down. To take advantage of the compact and cheap cooling method provided by Stirling cryocoolers, a direct, rigid, and thermally as well as mechanically stable fiber coupling of the QD emission to a single-mode fiber was developed.[33] This overcomes the drawback of low-frequency vibrations with the amplitude in the range of a few micrometers exceeding the size of the quantum emitter (at most tens of nanometers) inherent to the operation of the Stirling cryocooler. The proposed solution with superior performance is obtained by the interplay of various developed components, pump laser, growth of high-quality self-assembled QDs, and the design of a mesa-mirror-fiber-setup based on numerical modeling, deterministic fabrication of QD-mesas, advanced cooling method, specialty high-NA fiber, high-precision fiber positioning, and customized fiber components for spectral filtering. An important challenge of our device concept is to deliver the excitation efficiently and filter out the unwanted photons both from the pump laser and emitted from other parts of the structure. High isolation of the single transition is needed both in broad range as well as in a narrow range. Due to relatively small binding energies (in the range of 1 meV) of various excitonic complexes confined in the same QD,[37] a very sharp-edge band-pass filter is required. Even more important is the loss for the actual single-photon signal. Commercially available elements can offer arbitrary good isolation, but the insertion loss, especially if one has to stack several of such elements with different functionalities, is typically unacceptable with values in the range of 1.5 dB per element for a signal from a single QD. Therefore, minimizing the insertion loss of the fiber components was crucial for the realization of the reported source. This can be further optimized by using low loss splices instead of standard mating sleeves.

The achieved single-photon flux of the source in the range of 27–73 kHz, depending on the excitation conditions and required single-photon purity (down to 0.15), is far beyond the state-of-the-art for similar user-friendly sources: fiber-coupled and compact, not requiring any external filtering, but providing the end user with a train of single photons in a standard single-mode fiber at the output. At shorter wavelengths (about 900 nm), a multimode, fiber-coupled, and compact device was demonstrated.[32] It featured a photon flux of 230 kHz into the multimode optical fiber with $g^{(2)}(0) = 0.57$ under pulsed operation. In that case, the single-photon character of emission could be demonstrated under cw excitation with $g^{(2)}(0)$ equal to 0.07. When it comes to fiber-coupled, QD-based, single-photon sources at telecom

wavelengths, first results were reported by Xu et al.[14] However, this device was not fabricated deterministically and the reported results were obtained at 4.2 K while dipping the device in a liquid-helium storage dewar. For that source, the best obtained $g^{(2)}(0)$ was equal to 0.2 under cw excitation and the source efficiency was 3.75×10^{-5}. Therefore, when compared to the implementations above, the source reported here constitutes a substantial improvement over state-of-the-art of any known compact solutions.

The brightness of our single-photon source can certainly be further optimized as the probability to have a single photon per pulse is in the range of 1% currently. The achieved single-photon flux is modest yet, when compared to QD-based but non-compact sources at shorter wavelengths. However, the source characteristics of the latter were measured at temperatures below 10 K, that is, requiring complex liquid-helium-based experimental setups. In addition, external spectral filtering had to be used to select a single-photon transition, both making such a solution proof-of-principle like rather than an application-relevant device.

Photon fluxes achieved for QDs at shorter wavelengths (100 MHz[31] or 143 MHz[39]) for 0.5 GHz optical and electrical excitation show the high potential of QD-based single-photon sources. In principle, they outperform other (laser-based) approaches also at highly application-relevant telecom wavelengths. A low source efficiency in our case is mostly related to the non-ideal photon-extraction efficiency of the simple QD-micromesa and internal quantum efficiency of the emitter. Even for an ideal QD and the fully optimized mesa design, the maximum theoretically achievable outcoupling efficiency into the single-mode fiber is in the range of 20%.[35] Therefore, more sophisticated engineering of the photonic environment for maximizing the extraction efficiency, in particular, bulls-eye cavity designs for which efficiency exceeding 90% into low-NA collection optics is predicted,[40] might be used to improve it in the next development stages.

Applying a tunable narrow band-pass filter might also further increase the flexibility and functionality of the entire device concept. Also, for a good isolation of the single-photon emission from the scattered laser, the excitation wavelength has to be significantly different than the QD emission range (by at least 100 nm for our device). Therefore, the strictly resonant or even quasi-resonant excitation was at this stage not possible. It would also be less practical as a very specific different wavelength of the pump would be required for each QD and only one laser source could be used for each device, which would decrease the universal character of this design, and would also increase substantially the cost of the whole system, which is now mostly dictated by the Stirling cryocooler and the excitation source. One has to keep in mind that the coherence properties in the case of the investigated structures will be in any case limited by the operation temperature (40 K) and not by the non-resonant excitation scheme. On the other hand, it is straightforward to use our concept, which can easily be transferred to optical above-bandgap and wetting-layer excitation as well as electrically triggered structures where the pump rejection is not required at all, so it depends only on the availability of suitable QD emitters. The purity of the single photons is determined by the QD material itself. Thus, it is a matter of choosing a properly isolated transition with low emission background, which is not a limitation of the implemented concept itself, but relies more on the development of high-quality QD material at telecom wavelengths.[25]

4. Conclusion

We demonstrated a user-friendly, fully fiber-coupled triggered source of single photons in the telecom O-band suitable for applications in long-range quantum communication schemes. The single photons are emitted by a semiconductor QD, deterministically integrated into a micromesa and on-chip coupled to a high NA customized single-mode fiber. The QD sample is cooled by a compact Stirling cryocooler at 40 K. The main ingredient of the proposed solution are specially designed fiber components, the deterministic in situ fabrication of mesa structures following the numerically obtained structure design around the target QD and an ultra-precise interferometric method for fiber alignment (accuracy below 50 nm) with respect to the mesa center. Combining these developments resulted in a device performance with a probability of multiphoton events as low as 15% and the maximal single-photon generation rate at the single-mode fiber output of 73 kHz. The obtained rate of generation of single photons is by two orders of magnitude larger than the ≈0.7 kHz reported by Schlehahn et al.[32] for a multimode, fiber-coupled, stand-alone SPS based on a standard InGaAs QD emitting in the 900–950 nm wavelength range. This highlights the significant advances achieved in the present work, which not only provides a fully fiber-based solution, but also demonstrates single-mode operation in the O-band—all of which are crucial prerequisites for real-world device applications, for example, in the field of quantum communication. The long-term stability of the optical output of the stand-alone SPS is better than 1.5% (standard deviation). Our user-friendly device concept does not require a supply of cryogenic liquids; is robust; and provides a hardware solution being compact, mechanically stable, and portable. It does not require any additional adjustments or post selection of the single photons by the user as the filtering fiber systems are already integrated. Therefore, the end user can operate the source in a plug&play fashion, as at the output, it has a standard telecommunication single-mode fiber that delivers the train of triggered single photons at 1294.7 nm for the used QD. Noteworthy, our approach is independent of the material used and can be adapted to different spectral ranges. The limiting factors are the structural quality of the QD material and the spatial QD density. Additionally, the possibility of tuning the QD-based SPSs with external strain and static electric field[41,42] as well as electrical excitation[43] could be easily integrated in our source, rendering its application potential even larger. Therefore, these results pave the way to real-word application of QD-based fiber quantum networks.

5. Experimental Section

Sample Growth: The QDs were formed by self-organization during metalorganic chemical vapor deposition in the Stranski–Krastanov growth mode. Starting with a GaAs wafer, first, the bottom distributed Bragg reflector with 15 pairs of $GaAs/Al_{0.9}Ga_{0.1}As$ layers with 98.3/113.8 nm thickness on a 300 nm GaAs buffer was grown at 700 °C followed by a 505.4 nm thick additional GaAs layer. For the growth of the QD layer, the temperature

was decreased down to 500 °C. The active region constitutes of InGaAs QDs (formed from 2.5 monolayers (ML) of InGaAs with 66% In content and flushed with 1 ML of GaAs) and is followed by a 5.5 nm thick InGaAs strain-reducing layer with an In gradient from 30% at the bottom down to 10% at the top. After initial capping with 2 nm of GaAs, the final capping layer consisting of 612.7 nm of GaAs is grown at 615 °C.

In Situ Electron-Beam Lithography: The applied fiber positioning method[33,44] requires that a single QD is located with high accuracy in the center of a micrometer-sized nanophotonic structure. For that purpose, in situ electron-beam lithography (EBL)[45] optimized for 1.3 μm emission wavelength and with an overall positioning accuracy below 50 nm[34] was utilized. In this procedure 310 ± 2 nm of chemical semi amplified EBL resist (measured by ellipsometry) diluted to a solid content of 6.5% was spin coated on the sample surface. Next, the sample was mounted in the in situ EBL system and cooled down to cryogenic temperatures (15 K). At first, the cathodoluminescence mapping was performed with 40 ms integration time for each pixel to identify the most suitable QDs for further processing. The criteria at this step are the spatial isolation of the QD, the emission intensity, and the spectral range of emission. In this context, it is important to note that QD emission needs to fit within the bandwidth of the fiber band-pass filters which span in the range of 1293–1295 nm. The mapping dose must be below the onset dose for inverting the resist and in this particular processing, 8 mC cm^{-2} was used. After identifying a suitable QD, the lithography step was performed still at cryogenic temperatures within the same in situ EBL system. The resist was exposed using 25 mC cm^{-2} electron dose and single cylindrical mesa structures were patterned in each writing field. The nominal diameters of the mesas on this sample are 1050, 1075, and 1090 nm, and the mesa height (corresponding to etching depth) equals to 620 ± 5 nm. Further processing was performed at room temperature in the cleanroom. It included resist development and dry etching (reactive ion etching) of the patterned structures. Afterwards, scanning electron microscopy (SEM) in top-view configuration (no tilt angle) was performed to determine the actual mesa diameters and the etching depth was verified via profilometer measurements.

Positioning of the Fiber with Respect to the Mesa: For positioning of the optimized high-NA single-mode fiber with respect to the mesa center prior to gluing a zirconia ferrule with the fiber to the sample surface, an interferometric method detailed by Żołnacz et al.[33,44] was used. The alignment procedure was performed at room temperature which, importantly, does not rely on the actual QD signal (which is not detectable at room temperature), but takes advantage of the deterministic character of the mesa structure fabrication with a single QD in the center. The position of the fiber was adjusted for the center of the mesa based on measurements of the topography of the sample utilizing the interference between the spectrally broad signal from a supercontinuum light source reflected from the fiber facet and the surface of the sample dependent on the distance between the fiber and the sample surface. Both the fiber and the sample surface were first positioned horizontally using piezo actuators and the fiber was further moved across the sample surface at constant distance. The analysis of the spectral interference fringes allowed us to position the fiber with respect to the mesa center with 50 nm accuracy (for micromesas with diameters smaller than 2 μm), that is, with a deviation much smaller than the diameter (2.5 μm) of the single-mode fiber core. After having aligned the fiber with respect to the mesa center leaving an air gap between mesa and fiber end facet of about 0.5 μm, the fiber was set in physical contact with the sample surface which is crucial for long-term mechanical and thermal stability. Then the fiber ferrule was glued to the sample surface with ceramic UV-cured glue exhibiting a low thermal expansion coefficient of only 14 ppm $°C^{-1}$ (compared to the GaAs coefficient of 5.73 ppm $°C^{-1}$). It is important to note that this glue is not transparent in the spectral range of interest, so it was only applied outside the ferrule leaving the fiber end facet and the mesa top surface free of any glue.

Fiber Components: The fiber components specially designed for the presented single-photon source include a single-mode fiber with high (0.42) numerical aperture, broad band-pass filter to remove/suppress unwanted spontaneous emission background of the pulsed laser source, a fiber filter responsible for delivering the optical excitation to the sample (reflection channel) as well as spectrally suppressing it out from the detection path to provide high transmission for the actual QD signal (transmission channel), and finally a narrow band-pass filter (0.6 nm) for selecting the target emission line of the fiber-coupled QD. Additionally, the customized fiber coupled to the QD has to be spliced with a standard telecom fiber to provide an easy-to-integrate output of the device. The transmission of each component was evaluated with respect to the reference measurement in which a tested component was exchanged with a simple patch cord to account for spectral characteristics of the source and the detection system. Additionally, the noise level of the OSA itself was measured each time for illustrating the dynamic range of the detector to verify whether it is large enough or the result of the measurements constitutes only a lower limit of the isolation provided by the respective fiber element.

Table 1. Parameters of the specialty fiber filters.

Parameter	Pumping filter		Narrow band-pass filter
	Transmission channel	Reflection channel	
Maximal insertion loss [dB]	0.70	4.20 (single-mode) 1.80 (multimode)	0.50
Bandwidth [nm]	1150 ÷ 1600	785 ÷ 1000	Central wavelength ± 0.3
Laser attenuation [dB]	>40 (per chip)		>2.50

The customized fiber was optimized in terms of numerical aperture and residual thermal stress for safe operation at cryogenic temperatures. The high numerical aperture (NA = 0.42) was achieved by using a highly Ge-doped core with 40 mol% of GeO_2. Such a high level of doping results in a huge difference of thermal expansion coefficients between the core and the cladding of the fiber that might lead to fiber breaking either during fabrication of the fiber or cooling it down for low-temperature measurements of the QD signal. To reduce the stress level, a fiber with a three-step doping profile (40, 13, and 5 mol%), resulting in the similar refractive index profile (1:2:3 diameter ratios), was fabricated following the design obtained via the finite-element method simulations. This approach resulted in a numerical aperture of 0.42 with a cut-off wavelength for single-mode operation of 1050 nm for a fiber with 2.5 μm core diameter. The customized fiber was terminated with a zirconia ferrule polished into the spherical end-face. It was glued directly to the QD-micromesa and further sealed by an epoxy glue in a specially designed vacuum feedthrough to a portable Stirling cryocooler. The customized fiber has to be further spliced to a standard telecom single-mode fiber (core diameter of 9 μm) and the main challenge here is to overcome the 3.6 factor between the fiber core diameters. A low-loss splice (0.2 dB in both directions) was achieved using glass processing station with CO_2 laser splicer via the thermal core expansion technique that relies on equalizing the fiber core diameters by controlled heating of the splice area causing the GeO_2 dopant from the core to diffuse to the cladding, eventually creating a gradual low loss splice.

All filters were fabricated in the thin film filter (TFF) technology. The band-pass filters have a bandwidth of 0.6 nm with a flat-top characteristic that is important to maximize the emission line transmission through the filter. It is also possible to fabricate filters with a different bandwidth down to 0.3 nm (at the expense of higher loss of 1.2 dB). For their fabrication, a commercially available TFF chip was used and the central wavelength of the actual filter can be tuned by 2 nm via the angle of incidence on the chip that can be tuned on the fabrication stage of the filter. The tuning range of the central wavelength is limited by the change in the shape of the bandwidth and polarization selectivity appearing for high angles of incidence to 2 nm at maximum and 1 nm in practice. The parameters of the fiber filters are summed up in **Table 1**.

The characteristics of the fiber filters (see Figure 2) were measured using fiber-coupled supercontinuum light source (NKT Photonics SuperK Versa) and an OSA (Yokogawa AQ6370B) covering the spectral range of 600–1700 nm. The transmission of the filters was determined as a difference between the transmission of setup with the filter and a reference measurement in which the filter was replaced by a fiber patch cord. Additionally, the noise level of the OSA was measured showing in which cases the measurement results (in particular signal attenuation by the filter) are limited by the sensitivity of the detection system itself. In this case, only the lower limit for the attenuation can be determined due to limited dynamic range of the detector.

Experimental Setup—Spectroscopy Measurements: In general, two experimental configurations were used for the spectroscopy study of the SPS. The common part of the two configurations was the fiber-glued sample mounted in the Stirling cryocooler (base temperature 38 K) with optical excitation (laser output filtered with the broad band-pass filter) delivered via the customized fiber pumping filter. The non-resonant excitation of the investigated QD structures was realized using an electrically triggered, fiber-coupled, semiconductor diode laser that was custom-designed by PicoQuant. The laser was built around a preselected laser diode emitting at 805 nm. Special driving electronics permit freely selectable repetition rates up to 100 MHz using internal or even external triggering. The laser emits pulses with a pulse width of <50 ps (full width at half maximum) with average power of a few milliwatts, which can be further reduced by a built-in computer-controlled attenuator allowing to adjust the excitation power to the requirements of the QD structures. The difference in the two experimental configurations appears in the way the signal from the sample was filtered spectrally. For the pre-characterization of emission from the sample, the optical signal was out-coupled from the output port of the fiber filter for pumping to free space and filtered spectrally via a 0.32 m focal length spectrometer with 600 grooves mm^{-1} grating blazed at 1000 nm, providing 0.4 nm bandwidth at its output. The PL signal was further coupled to the single-mode fiber connected to a single-photon counting module (superconducting NbN nanowire detector with 20% quantum efficiency—SNSPD). This configuration was used to measure PL spectra of the QD in a broad spectral range to identify proper excitation conditions for autocorrelation measurements and, in particular, to select a proper band-pass filter for the second, all-fiber configuration. For the measurements on the actual fully fiber-coupled device, the output of the pumping filter was connected to the narrow band-pass filter and further via the output connector of the stand-alone SPS to a 50:50 beam splitter based on single-mode fibers. Each output of the beam splitter was then connected to a SNSPD for autocorrelation measurements that were carried out using a multichannel picosecond event timer (PicoHarp 300) with 256 ps time-bin width. The measured histograms were fitted with the following function[17]

$$g^{(2)}_{\text{fit}}(\tau) = g_{\text{bg}} + g_{\text{auto}} f(|\tau|) + \sum_{n\neq 0} f\left(\left|\tau - nT_0\right|\right) \quad (1)$$

where g_{bg} corresponds to the background counts, g_{auto} indicates figure of merit—$g^{(2)}(0)$, and $f(\tau)$ is the normalized biexponential function with T_0 being the distance between the consecutive pulses (corresponding to the repetition rate of the excitation laser) that describe the autocorrelation between the photons emitted within different pulses. The peak height for the non-zero delay peaks determined from the fitting procedure was further used to normalize the coincidence events histogram to obtain the time delay-dependent second-order correlation function $g^{(2)}(\tau)$.

Acknowledgements

This work was funded by the FI-SEQUR project jointly financed by the European Regional Development Fund (EFRE) of the European Union in the framework of the programme to promote research, innovation, and technologies (Pro FIT) in Germany, and the National Centre for Research and Development in Poland within the 2nd Poland-Berlin Photonics Programme, grant number 2/POLBER-2/2016 (project value 2 089 498 PLN). Support from the German Science Foundation via CRC 787, from the Federal Ministry of Education and Research, BMBF, grant number 05M20ZBM, and from the Polish National Agency for Academic Exchange is also acknowledged.

Conflict of Interest

The authors declare no conflict of interest.

Keywords

III-V semiconductor epitaxial quantum dots, fiber elements design and fabrication, photon statistics, quantum communication, quantum-dot-based devices, quantum optics, single-photon sources

Received: February 10, 2020
Revised: March 26, 2020
Published online: May 11, 2020

[1] D. Bouwmeester, A. Ekert, A. Zeilinger, *The Physics of Quantum Information*, Springer, Berlin **2000**.
[2] N. Sangouard, C. Simon, J. Minář, H. Zbinden, H. de Riedmatten, N. Gisin, *Phys. Rev. A* **2007**, *76*, 050301.
[3] H. J. Kimble, *Nature* **2008**, *453*, 1023.
[4] J. L. O'Brien, *Science* **2007**, *318*, 1567.
[5] D. J. Brod, E. F. Galvão, A. Crespi, R. Osellame, N. Spagnolo, F. Sciarrino, *Adv. Photonics* **2019**, *1*, 034001.
[6] T. Heindel, C. A. Kessler, M. Rau, C. Schneider, M. Fürst, F. Hargart, W.-M. Schulz, M. Eichfelder, R. Roßbach, S. Nauerth, M. Lermer, H. Weier, M. Jetter, M. Kamp, S. Reitzenstein, S. Höfling, P. Michler, H. Weinfurter, A. Forchel, *New J. Phys.* **2012**, *14*, 083001.
[7] M. Lucamarini, Z. L. Yuan, J. F. Dynes, A. J. Shields, *Nature* **2018**, *557*, 400.
[8] M. Sasaki, M. Fujiwara, H. Ishizuka, W. Klaus, K. Wakui, M. Takeoka, S. Miki, T. Yamashita, Z. Wang, A. Tanaka, K. Yoshino, Y. Nambu, S. Takahashi, A. Tajima, A. Tomita, T. Domeki, T. Hasegawa, Y. Sakai, H. Kobayashi, T. Asai, K. Shimizu, T. Tokura, T. Tsurumaru, M. Matsui, T. Honjo, K. Tamaki, H. Takesue, Y. Tokura, J. F. Dynes, A. R. Dixon et al., *Opt. Express* **2011**, *19*, 10387.
[9] H.-L. Yin, T.-Y. Chen, Z.-W. Yu, H. Liu, L.-X. You, Y.-H. Zhou, S.-J. Chen, Y. Mao, M.-Q. Huang, W.-J. Zhang, H. Chen, M. J. Li, D. Nolan, F. Zhou, X. Jiang, Z. Wang, Q. Zhang, X.-B. Wang, J.-W. Pan, *Phys. Rev. Lett.* **2016**, *117*, 190501.
[10] R. Dixon, Z. L. Yuan, J. F. Dynes, A. W. Sharpe, A. J. Shields, *Opt. Express* **2008**, *16*, 18790.
[11] X.-S. Ma, T. Herbst, T. Scheidl, D. Wang, S. Kropatschek, W. Naylor, B. Wittmann, A. Mech, J. Kofler, E. Anisimova, V. Makarov, T. Jennewein, R. Ursin, A. Zeilinger, *Nature* **2012**, *489*, 269.
[12] S.-K. Liao, W.-Q. Cai, J. Handsteiner, B. Liu, J. Yin, L. Zhang, D. Rauch, M. Fink, J.-G. Ren, W.-Y. Liu, Y. Li, Q. Shen, Y. Cao, F.-Z. Li, J.-F. Wang, Y.-M. Huang, L. Deng, T. Xi, L. Ma, T. Hu, L. Li,. N.-L. Liu, F. Koidl, P. Wang, Y.-A. Chen, X.-B. Wang, M. Steindorfer, G. Kirchner, C.-Y. Lu, R. Shu, R. Ursin et al., *Phys. Rev. Lett.* **2018**, *120*, 030501.
[13] L. Schweickert, K. D. Jöns, K. D. Zeuner, S. F. Covre da Silva, H. Huang, T. Lettner, M. Reindl, J. Zichi, R. Trotta, A. Rastelli, V. Zwiller, *Appl. Phys. Lett.* **2018**, *112*, 093106.
[14] X. Xu, F. Brossard, K. Hammura, D. A. Williams, B. Alloing, L. H. Li, A. Fiore, *Appl. Phys. Lett.* **2008**, *93*, 021124.

[15] M. B. Ward, O. Z. Karimov, D. C. Unitt, Z. L. Yuan, P. See, D. G. Gevaux, A. J. Shields, P. Atkinson, D. A. Ritchie, *Appl. Phys. Lett.* **2005**, *86*, 201111.
[16] C. Zinoni, B. Alloing, C. Monat, V. Zwiller, L. H. Li, A. Fiore, L. Lunghi, A. Gerardino, H. de Riedmatten, H. Zbinden, N. Gisin, *Appl. Phys. Lett.* **2006**, *88*, 131102.
[17] T. Miyazawa, K. Takemoto, Y. Nambu, S. Miki, T. Yamashita, H. Terai, M. Fujiwara, M. Sasaki, Y. Sakuma, M. Takatsu, T. Yamamoto, Y. Arakawa, *Appl. Phys. Lett.* **2016**, *109*, 132106.
[18] M. Paul, J. Kettler, K. Zeuner, C. Clausen, M. Jetter, P. Michler, *Appl. Phys. Lett.* **2015**, *106*, 122105.
[19] Ł. Dusanowski, P. Holewa, A. Maryński, A. Musiał, T. Heuser, N. Srocka, D. Quandt, A. Strittmatter, S. Rodt, J. Misiewicz, S. Reitzenstein, G. Sęk, *Opt. Express* **2017**, *25*, 31122.
[20] M. Benyoucef, M. Yacob, J. P. Reithmaier, J. Kettler, P. Michler, *Appl. Phys. Lett.* **2013**, *103*, 162101.
[21] A. Musiał, P. Holewa, P. Wyborski, M. Syperek, A. Kors, J. P. Reithmaier, G. Sęk, M. Benyoucef, *Adv. Quantum Technol.* **2020**, *3*, 1900082.
[22] S. L. Portalupi, M. Jetter, P. Michler, *Semicond. Sci. Technol.* **2019**, *34*, 053001.
[23] P. Michler, *Quantum Dots for Quantum Information Technologies*, Springer, Cham, Switzerland **2017**.
[24] P. Lodahl, *Quantum Sci. Technol.* **2018**, *3*, 013001.
[25] X. Cao, M. Zopf, F. Ding, *J. Semicond.* **2019**, *40*, 071901.
[26] A. Muller, H. Zbinden, N. Gisin, *Europhys. Lett.* **1996**, *33*, 335.
[27] S. Wengerowsky, S. K. Joshi, F. Steinlechner, J. R. Zichi, S. M. Dobrovolskiy, R. van der Molen, J. W. N. Los, V. Zwiller, M. A. M. Versteegh, A. Mura, D. Calonico, M. Inguscio, H. Hübel, L. Bo, T. Scheidl, A. Zeilinger, A. Xuereb, R. Ursin, *Proc. Natl. Acad. Sci. USA* **2019**, *116*, 6684.
[28] A. Boaron, G. Boso, D. Rusca, C. Paul Vulliez, C. Autebert, M. Caloz, M. Perrenoud, G. Gras, F. Bussières, M.-J. Li, D. Nolan, A. Martin, H. Zbinden, *Phys. Rev. Lett.* **2018**, *121*, 190502.
[29] G. Brassard, N. Lütkenhaus, T. Mor, B. C. Sanders, *Phys. Rev. Lett.* **2000**, *85*, 1330.
[30] Z. Xiang, J. Huwer, R. M. Stevenson, J. S. Szymanska, M. B. Ward, I. Farrer, D. A. Ritchie, A. J. Shields, presented at Conf. on Lasers and Electro-Optics, OSA Technical Digest, CLEO: QELS_Fundamental Science 2019, San Jose, California United States, 5–10 May 2019, paper FM4C.6.
[31] Quandela homepage, http://quandela.com/ (accessed: December 2019).
[32] A. Schlehahn, S. Fischbach, R. Schmidt, A. Kaganskiy, A. Strittmatter, S. Rodt, T. Heindel, S. Reitzenstein, *Sci. Rep.* **2018**, *8*, 1340.
[33] K. Żołnacz, A. Musiał, N. Srocka, J. Große, M. J. Schlösinger, P.-I. Schneider, O. Kravets, M. Mikulicz, J. Olszewski, K. Poturaj, G. Wójcik, P. Mergo, K. Dybka, M. Dyrkacz, M. Dłubek, S. Rodt, S. Burger, L. Zschiedrich, G. Sęk, S. Reitzenstein, W. Urbańczyk, *Opt. Express* **2019**, *27*, 26772.
[34] N. Srocka, A. Musiał, P.-I. Schneider, P. Mrowiński, P. Holewa, S. Burger, D. Quandt, A. Strittmatter, S. Rodt, S. Reitzenstein, G. Sęk, *AIP Adv.* **2018**, *8*, 085205.
[35] P.-I. Schneider, N. Srocka, S. Rodt, L. Zschiedrich, S. Reitzenstein, S. Burger, *Opt. Express* **2018**, *26*, 8479.
[36] P.-I. Schneider, X. G. Santiago, V. Soltwisch, M. Hammerschmidt, S. Burger, C. Rockstuhl, *ACS Photonics* **2019**, *6*, 2726.
[37] P. Mrowiński, A. Musiał, K. Gawarecki, Ł. Dusanowski, T. Heuser, N. Srocka, D. Quandt, A. Strittmatter, S. Rodt, S. Reitzenstein, G. Sęk, *Phys. Rev. B* **2019**, *100*, 115310.
[38] M. Pelton, C. Santori, J. Vuckovic, B. Zhang, G. S. Solomon, J. Plant, Y. Yamamoto, *Phys. Rev. Lett.* **2002**, *89*, 233602.
[39] A. Schlehahn, M. Gaafar, M. Vaupel, M. Gschrey, P. Schnauber, J.-H. Schulze, S. Rodt, A. Strittmatter, W. Stolz, A. Rahimi-Iman, T. Heindel, M. Koch, S. Reitzenstein, *Appl. Phys. Lett.* **2015**, *107*, 041105.
[40] L. Rickert, T. Kupko, S. Rodt, S. Reitzenstein, T. Heindel, *Opt. Express* **2019**, *27*, 36824.
[41] B. Höfer, F. Olbrich, J. Kettler, M. Paul, J. Höschele, M. Jetter, S. L. Portalupi, F. Ding, P. Michler, O. G. Schmidt, *AIP Adv.* **2019**, *9*, 085112.
[42] Z.-H. Xiang, J. Huwer, J. Skiba-Szymanska, R. M. Stevenson, D. J. P. Ellis, I. Farrer, M. B. Ward, D. A. Ritchie, A. J. Shields, arXiv:1909.12222, **2019**.
[43] M. B. Ward, T. Farrow, P. See, Z. L. Yuan, O. Z. Karimov, A. J. Bennett, A. J. Shields, P. Atkinson, K. Cooper, D. A. Ritchie, *Appl. Phys. Lett.* **2007**, *90*, 063512.
[44] K. Żołnacz, W. Urbańczyk, N. Srocka, T. Heuser, D. Quandt, A. Strittmatter, S. Rodt, S. Reitzenstein, A. Musiał, P. Mrowiński, G. Sęk, K. Poturaj, G. Wójcik, P. Mergo, K. Dybka, M. Dyrkacz, M. Dłubek, *Proc. SPIE* **2018**, *10674*, 106741R.
[45] M. Gschrey, A. Thoma, P. Schnauber, M. Seifried, R. Schmidt, B. Wohlfeil, L. Krüger, J.-H. Schulze, T. Heindel, S. Burger, F. Schmidt, A. Strittmatter, S. Rodt, S. Reitzenstein, *Nat. Commun.* **2015**, *6*, 7662.